Perovskite-Based Nanocomposite Electrocatalysts: An Alternative to Platinum ORR Catalyst in Microbial Fuel Cell Cathodes

Gopa Nandikes [1], Shaik Gouse Peera [2,*] and Lakhveer Singh [1,*]

[1] Department of Environmental Science, SRM University-AP, Amaravati 522502, Andhra Pradesh, India; gopanandikes_p@srmap.edu.in
[2] Department of Environmental Science, Keimyung University, Daegu 42601, Korea
* Correspondence: gouse@kmu.ac.kr (S.G.P.); Lakhveer.s@srmap.edu.in (L.S.)

Abstract: Microbial fuel cells (MFCs) are biochemical systems having the benefit of producing green energy through the microbial degradation of organic contaminants in wastewater. The efficiency of MFCs largely depends on the cathode oxygen reduction reaction (ORR). A preferable ORR catalyst must have good oxygen reduction kinetics, high conductivity and durability, together with cost-effectiveness. Platinum-based electrodes are considered a state-of-the-art ORR catalyst. However, the scarcity and higher cost of Pt are the main challenges for the commercialization of MFCs; therefore, in search of alternative, cost-effective catalysts, those such as doped carbons and transition-metal-based electrocatalysts have been researched for more than a decade. Recently, perovskite-oxide-based nanocomposites have emerged as a potential ORR catalyst due to their versatile elemental composition, molecular mechanism and the scope of nanoengineering for further developments. In this article, we discuss various studies conducted and opportunities associated with perovskite-based catalysts for ORR in MFCs. Special focus is given to a basic understanding of the ORR reaction mechanism through oxygen vacancy, modification of its microstructure by introducing alkaline earth metals, electron transfer pathways and the synergistic effect of perovskite and carbon. At the end, we also propose various challenges and prospects to further improve the ORR activity of perovskite-based catalysts.

Keywords: oxygen reduction reaction; perovskite; cathode; microbial fuel cell

1. Introduction

Energy plays a vital role in the modern era as there is an excess need for energy due to rapid industrialization and the increased global population. Increasing energy demands trigger substantial research to explore cost-effective renewable energy building technologies with improved efficiency [1]. The prevalence of pollutants in aquatic systems and wastewater is another serious concern due to their negative impact on the environment and ecosystems [2]. Microbial fuel cells (MFCs) are considered a favorable technology for simultaneous wastewater treatment together with bioelectricity generation, as they can use wastewater as a source for producing bioenergy [3,4]. Sharing the similar working principle of electrochemistry with common fuel cells, an MFC is designed to have a set of anode–cathode segments [5]. In MFCs, the electrochemically active microorganisms, also called exoelectrogens, attach to the anode and metabolize organic matter in the wastewater to produce electrons and protons. As a result of microbial respiration, electrons are generated and they are transferred to the anode electrode, which further performs the electrical work by passing through the circuit, and protons are transferred to the cathode via a proton exchange membrane. At the cathode, the protons and electrodes are combined in the presence of oxidants such as oxygen to generate water as the final product [6]. By this combined bio–electrocatalytic reaction, the wastewater is treated at the anode, together

with the useful energy output (Figure 1). Membrane-free MFCs are proven to be more efficient and cost-effective, but there are a few challenges, such as the reduced coulombic efficiency, distance between the electrodes and limitations in the design of single-chambered MFCs (SCMFCs). Proton exchange membranes such as Nafion 117, which is expensive, have been replaced by sulfonated polyether ether ketone (SPEEK) [7], sulfonated SiO_2 and sulfonated polystyrene ethylene butylene polystyrene (SSEBS), etc. [8]. These membranes can overcome the limitations and even provide better outputs, as indicated in recent studies [9,10]. The performance of MFCs is reliant on several factors, such as the type of electrode material at the anode, the type of exoelectrogens in the wastewater, the type and efficiency of the cathode, enzymes and operational conditions [2,7,11,12]. The capability of a cathode for reduction reactions is an important aspect for the overall energy output from the microbial fuel cell. A vast number of cathode materials have been tried and tested in MFCs, in which perovskite-based nanocomposite electrocatalysts have gained much attention in recent times. This study reviews the perovskite electrocatalysts that have been used in the MFC system, their unique reaction pathway and the feasibility of maximizing the energy output through changes in perovskite's elemental type and composition.
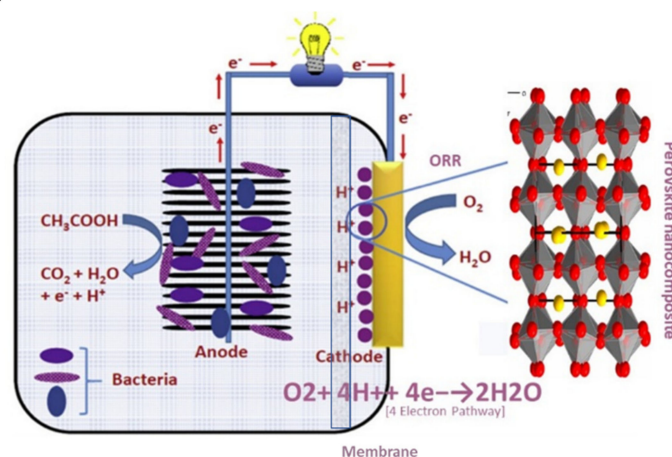
Figure 1. Graphical representation of a single-chambered MFC with perovskite ORR catalyst having a four-electron pathway.

2. ORR Catalysts

There are various elements in MFCs that pertain to their efficiency. Among all, the type of anode electrode and efficient ORR cathode electrocatalysts are believed to be the most influential factors, which decide the practical power generation capacity of MFCs [13]. In particular, a highly catalytically active ORR cathode catalyst is essential for the continuous generation of bioenergy. An ideal ORR catalyst must be relatively affordable, abundant, environmentally safe and maintain consistent catalytic activity and stability [14]. The cathodic ORR should ideally result in direct four-electron transfer, in contrast to the undesirable two-electron process [15]. Generally, electrocatalysts that contain noble metals such as Pt follow a direct four-electron transfer reaction, whereas electrocatalysts made up of transition metals such as Co, Fe, Mn, Ni, etc., follow a dominant four-electron pathway or a mixed two- and four-electron pathway. A two-electron pathway results in a lower electron transfer rate and onset potential, therefore leading to a considerable energy loss [14–16].

2.1. Pt-Based Catalyst

For decades, the platinum catalyst has been known to be the most ideal catalyst for bio–electrochemical cells, especially MFCs [17]. Even though the Pt catalyst is considered a highly active solution and a benchmark for ORR catalysts, its major drawback is its high cost and limited availability [6]. In addition, Pt-based catalysts are susceptible to catalytic poisoning and a loss in activity, and the stability decreases over time. Hence, research has shifted to explore low-cost metals and efficient materials to be used as ORR catalysts [18].

2.2. Non-Pt-Based Catalysts

In recent years, non-precious metals have been tested as possible options for ORR catalysts in MFCs. Platinum group metal-free (PGM-free) catalysts are a class of catalysts that include transition metals (Fe, M, Mn, Cu) [19–21] and heteroatom-doped carbon-based materials. Ideally, most of these catalysts have confirmed excellent electrocatalytic activity. In particular, activated carbon [21,22], graphite [23,24], carbon nanotubes [25], nitrogen-doped carbon and carbon black [26] have achieved vast recognition due to their increased surface area and electrical conductivity. Biochar has been used as an ORR catalyst lately due its availability, cost-effectiveness and ideal physical and chemical characteristics [23]. Biochar's properties assists in major nutrient cycles in microorganisms and improve their growth [27–29]. Transition metal oxides (TMOs) constitute a broad family of electrocatalysts that constitutes single- and mixed-metal oxides [30]. When compared to Pt-based catalysts, TMO-based catalysts have several advantages, such as being economical and more abundant, ease of synthesis and eco-friendliness [31]. Transition metal oxides acquire multiple valence states, which results in a variety of oxides having distinctive crystal structures. Transition metals of VII and VIII group elements have multiple valences and several oxides, enabling them to have various electrocatalytic applications [32–38].

2.2.1. Single-Metal Oxides

Generally, single-metal oxides have less electrical conductivity. Hence, providing them with a conductive substrate or matrixes such as carbon or graphene material have proven to be crucial in raising their catalytic performance.

Manganese oxides such as $Mn_2O_{5-\delta}$ have gathered attention as a demanding single-metal oxide catalyst because of their variable valence states and variable structures, proving their exceptional redox electrochemistry. Manganese oxides can function simultaneously as an ORR as well as OER catalyst [34], thus making them an interesting bifunctional catalyst for oxygen electrochemistry. Recently, the introduction of oxygen vacancies into the Mn oxide was found to be an efficient strategy to further improve the ORR activity of Mn-oxide-based catalysts, which increased the proportion of more active Mn^{3+} and increased the electrical conductivity. Nevertheless, the ORR activity of Mn-based oxides overall has been either similar or, in some cases, better than that of Pt/C [38].

Cobalt oxide is another good candidate for ORR that has several advantages over other oxide candidates because of its tunable composition, high electrocatalytic activity and low cost [35]. Co_3O_4 has a spinel structure, where Co^{2+} and Co^{3+} act as a redox couple and occupy tetrahedral and octahedral voids to facilitate electron transfer; in particular, the exposure of active Co^{3+} is found to play a key role in the ORR reaction [36].

Vanadium pentoxide (V_2O_5) has been successfully used as an alternative to platinum cathode catalysts in a single-chambered MFC. V_2O_5 was synthesized through a hydrothermal method and electrochemical measurements proved that V_2O_5 is comparable in performance by up to 55% to that of Pt/C [31].

2.2.2. Mixed-Metal Oxides

Mixed-metal oxides are an amalgam of stable metals, which can be bi-metal, tri-metal, or multi-metal systems. These metals possess different valence states and have been used extensively used as ORR catalysts [39]. Within the mixed-metal oxides category, spinel-type oxides and perovskite oxides are the most investigated systems.

Spinel-Type Oxides

These fall within the category of mixed-metal oxides having a AB_2O_4 chemical formula, where A is taken as a divalent metal ion such as Mg, Co, Ni, Zn, Fe or Mn. A trivalent metal ion is used as the B element, such as Cr, Mn, Co, Al or Fe. Cations of different valency states help in reducing the activation energy associated with the electron exchange reaction by the hopping process during the ORR reaction. Ideal spinel structures are cubical with closely packed oxides, besides the two tetrahedral and the four octahedral points in the formula

unit. B^{3+} ions occupy four octahedral sites and A^{2+} occupy the two tetrahedral sites. This type of structure is called a "normal spinel". If B^{3+} ions take up all the tetrahedral sites and a pair of the octahedral sites, and the remaining octahedral sites are occupied by A^{2+} ions, then it is called an "inverse spinel" structure [40–43].

3. Perovskite Oxides

The perovskite oxides are a family of mixed-metal oxides with a general compositional formula of ABO_3, in which A-site elements are of rare earth and alkaline earth elements, whereas the B site constitutes a transition element. Perovskites are best known for their advantages of substituting A- or B-site cations to produce active and stable electrocatalysts [41]. This substitution of A or B sites with various atoms introduces abundant oxygen vacancies in the anion network, which helps oxygen molecules to bond together during ORR. Various elements can be introduced in the perovskite oxide's B site and can be altered on the basis of structure and composition in order to enhance the electrical conductivity and oxygen vacancy of the perovskites [43]. Thus, indicating a suitable transition metal at the B site can prevent the morphological deformation of the high oxygen vacancy and gives an optimal D band center for the whole B site [44,45]. This will enhance the overall catalytic performance of perovskite composites (Figure 2).
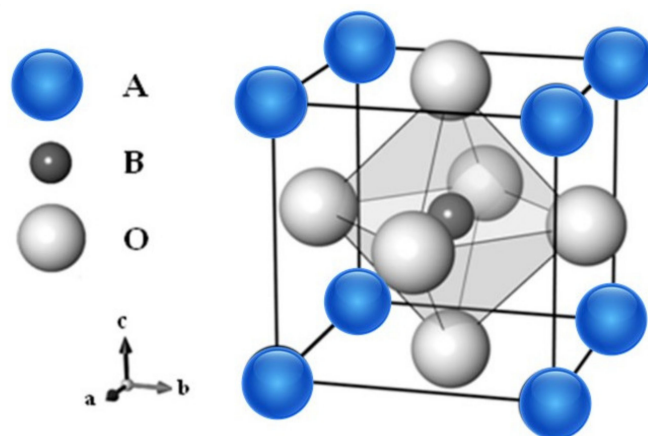
Figure 2. Crystal structure of perovskite oxide with ABO_3 composition. (Concept adopted with permission from [43]. Copyright 2020, MDPI, Open Access).

Perovskite oxides have a cubic structure in which A atoms occupy the corners of the cubic cell. In the central six-fold coordination, there are B atoms occupied by an octahedron of six anions, with the O_2 atoms situated in the center of the faces [44]. The B site is comparatively smaller than the A-site cation. Apart from the simple perovskite ABO_3 structure, modification can be achieved by integrating two different kinds of B ions with separate charge and proportion. Equiatomic portions of two different ions in the B site are often replaced, making the formula of the perovskite $ABB'O_6$. The two developed B ion units can be observed as doubled within the three axes. In most cases, B and B' charges may be different. In this scenario, oxygen atoms marginally shift towards the more charged ones. However, this process does not alter the octahedral symmetry of the perovskite [45].

3.1. ORR Mechanism of Perovskite-Type Oxides

Typically, ORR takes place through two types of pathways, either a direct four-electron reduction pathway or an indirect 2 + 2 electron reduction pathway into two water molecules in an acidic environment or four OH in an alkaline medium. A direct four-electron reduction is highly required to maintain the high energy output.

Alkaline electrolyte $4e^-$ pathway:

$$O_2 + 2H_2O + 4e^- \rightarrow 4OH^-$$
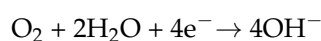
Acidic electrolyte $4e^-$ pathway:

$$O_2 + 4H^+ + 4e^- \rightarrow 2H_2O$$
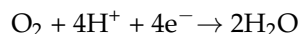
Perovskites are known to perform a direct four-electron reduction of O_2 to four OH^- ions. If the ORR takes place through a two-electron reduction process, it leads to the formation of undesired H_2O_2 and HO^{2-}. Jin et al. [46] proposed a possible catalytic ORR cycle in alkaline medium on a perovskite catalyst, as shown in Figure 3.
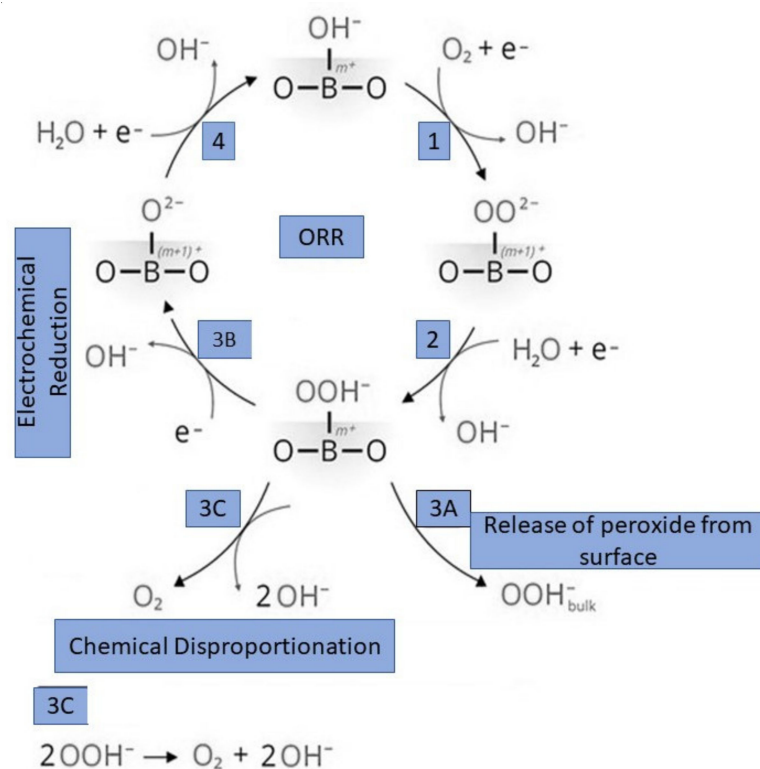
Figure 3. Representation of ORR mechanism in perovskite. (**1**) represents the initial step of ORR with adsorption of O_2 on B site, (**2**) peroxide formation with addition of proton in O_2, (**3A**) release of peroxide from surface, (**3B**) electrochemical reduction, (**3C**) chemical disproportionation. (Reprinted with permission from [47]. Copyright 2021, ACS Publications, Open Access).

Due to the abundance of OH^- ions in an alkaline environment, the perovskite's surface is always adsorbed and covered by OH^- ions at the B site. The first step in the ORR process is the adsorption of O_2 at the B site by replacing the pre-adsorbed OH^- ion in the presence of one electron (Figure 3) [47]. In the associative ORR reduction pathway, it is the B site of the ABO_3 perovskite onto which O_2 is adsorbed. The second step would be the addition of a proton to the previously adsorbed O_2 to form a peroxide (OOH^-). In a consecutive reaction of OOH^- at the B site, there would be three possibilities: (3A) the formed OOH^- can desorb from the B site and enter the bulk solution; (3B) two OOH^- on nearby sites would collectively undergo the hydrogen peroxide chemical disproportionation (HPCD) reaction to form two OH^- and one O_2 molecule; (3C) the most desirable reaction, in which OOH^- undergo reduction electrochemically (hydrogen peroxide electrochemical reduction reaction (HPER)) to form O^{2-}, which further reacts with H_2O and e^- to form OH^-, completing the one cycle of ORR. The selectivity of the OOH^- reaction among the three possibilities depends on the composition of perovskites and electrode parameters [48]. In order to quantify the electron transfer rates and to distinguish two-electron and four-electron pathways, a rotating ring disk electrode (RRDE) is used. It recognizes the electrons exchanged by counting the hydroperoxides found at the ring [49,50].

3.2. Application of Perovskite-Based ORR Electrode in MFCs

Based on the above knowledge, various researchers have developed a variety of perovskite-based catalysts for ORR and for application in MFCs. In a study by F. Shahbazi Farahani and group [51], the authors developed a bimetallic Fe-Mn perovskite-type oxide supported on carbon Vulcan ($C/FeMnO_3$) and graphene oxide ($GO/FeMnO_3$) by a chemical/thermal reduction method. The produced bimetallic $FeMnO_3$ phase having the perovskite structure was found to be homogeneously dispersed on the carbon support. $GO/FeMnO_3$ and $C/FeMnO_3$ composites exhibited good catalytic activity towards ORR both in alkaline and acidic environments, as depicted by hydrodynamic voltammetry, RRDE, cyclic voltammetry and EIS. The ORR charge transfer resistance of $C/FeMnO_3$ was found to be much lower than that of $GO/FeMnO_3$, signifying a low ORR kinetic rate for $GO/FeMnO_3$ (Figure 4). This is due to the restacking of graphene oxide sheets during the formation of the catalyst, which affected both the available metal oxides and the metal-oxide-assisted interaction negatively. In a typical setup, MFCs should be able to work in variable process states in terms of functioning and also fuel composition. Catalysts should be able to cope with the changes and show stable results. Hence, the authors conducted an accelerated stress test, in which $C/FeMnO_3$ presented excellent stability in simulated conditions. The kinetic data in terms of power and voltage displayed better performance than that of the Pt-based MFC. Despite these findings, the longevity of these metal oxides with carbon hybrids is, however, a concern that needs further study [51].
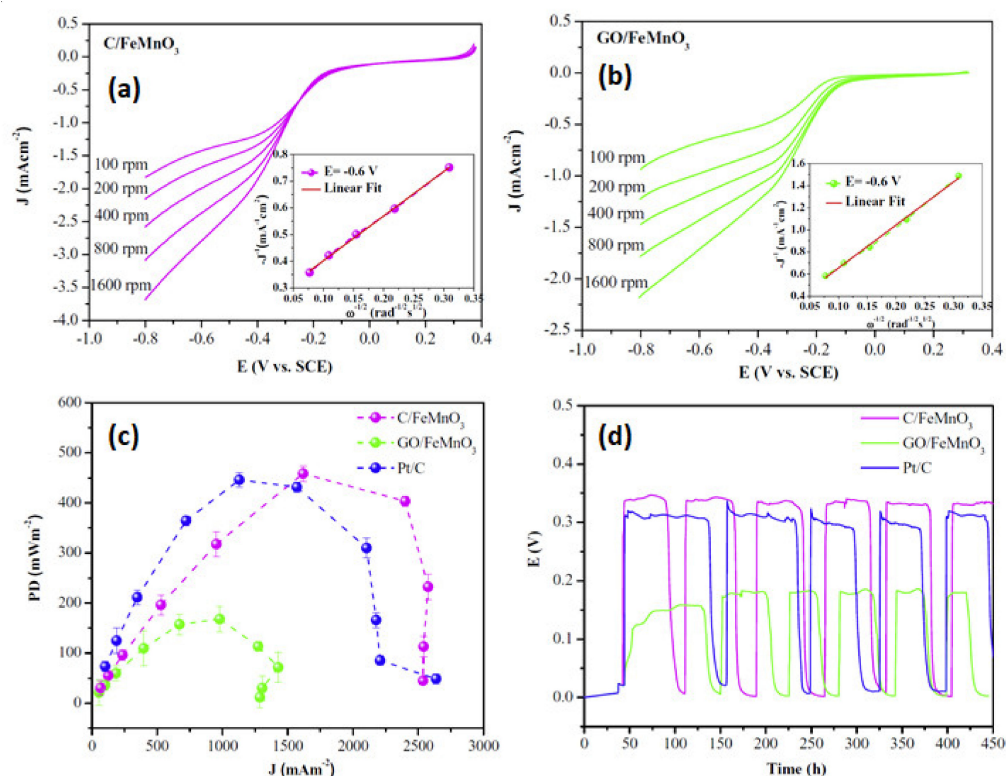
Figure 4. LSV curves at different electrode rotation rates of (**a**) $C/FeMnO_3$ and (**b**) $GO/FeMnO_3$ in O_2-saturated neutral PBS (scan rate:10 mVs^{-1}), with Koutecky–Levich plots obtained at ~0.6 V as an inset; (**c**) polarization and power density (PD) curves of MFCs assembled with $C/FeMnO_3$, $GO/FeMnO_3$ and Pt/C cathodes fed with 1 mgL^{-1} sodium acetate in neutral PBS; (**d**) voltage cycles under 1 kΩ external resistance as a function of time. (Reprinted with permission from [51]. Copyright 2019, Elsevier).

In a recent study [52], a Zn doping strategy was used to alter the microstructure and produce oxygen vacancies on perovskite in an attempt to enhance the ORR activity (Figure 5). Zn was doped together with iron to form a $CaFe_{0.7}Zn_{0.3}O_3$ perovskite oxide

that showed good catalytic activity, with a porous structure and improved surface area. Moreover, Zn and Fe showed an impressive synergy in improving the formation of oxygen vacancies, together with the formation of a mixed valence state of Fe^{2+}/Fe^{3+}. Zn-doped perovskite oxides ($CaFe_{0.7}Zn_{0.3}O_3$) displayed excellent ORR kinetics, onset potential (0.194 V vs. Ag/AgCl), and half-wave potential (−0.219 V vs. Ag/AgCl) in alkaline conditions, outperforming the Pt/C ORR catalyst. This exemplary performance is likely due to three main factors, one being the doping of the Zn element uniformly in the perovskite oxide. This leads to the generation of mesoporous pores via high-temperature carbonization evaporating the Zn in the mixture, forming a hierarchically porous assembly. The second is B-site doping with Zn ions, which creates more oxygen vacancies by elevating the oxygen unavailability rates and increasing the conductivity. The third important factor is the mixed valence state of Fe^{2+}/Fe^{3+}, which helps to stabilize the perovskite's catalytic activity, in addition to the presence of the Fe_3C active phase in the catalyst. Moreover, $CaFe_{0.7}Zn_{0.3}O_3$ follows the ideal four-electron pathway of ORR, which delivered a maximum power density of 892 mWm^{-3} with excellent stability over 160 h of operation time. The inferences from the study confirm the feasibility of the $CaFe_{0.7}Zn_{0.3}O_3$ catalyst as a substitution for a Pt cathode catalyst [52].
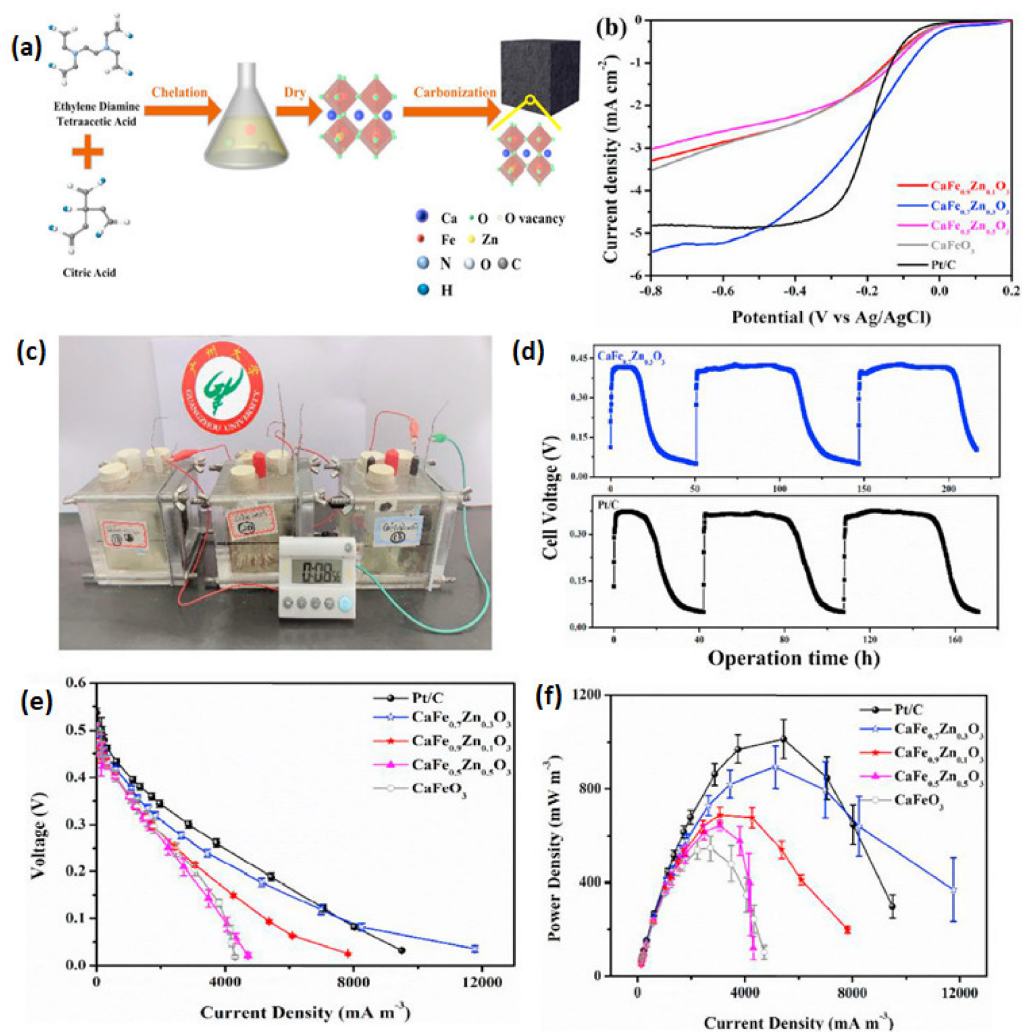
Figure 5. (**a**) The fabrication process of $CaFe_xZn_{(1-x)}O_3$ catalysts; (**b**) electron transfer number and H_2O_2 yield of $CaFe_{0.7}Zn_{0.3}O_3$; (**c**) simulated operation of MFCs; (**d**) output voltage of $CaFe_{0.7}Zn_{0.3}O_3$ and Pt/C; (**e**) polarization curves; (**f**) power density of $CaFe_{0.7}Zn_{0.3}O_3$ and Pt/C. (Reprinted with permission from [52]. Copyright 2021, Elsevier).

F. Nourbakhsh et al. [5] used $LaCoO_3$ (LC), $LaMnO_3$ (LM) and $LaCo_{0.5}Mn_{0.5}O_3$ (LMC) perovskite oxide nanoparticle-based cathode catalysts as a substitute for a platinum cathode (Figure 6). The Lanthanum-based perovskite-type oxide cathode catalysts produced were tested for their catalytic efficiency in a dual-chambered MFC. The LC, LM and LMC were tested individually for their morphology, structure and electrochemical properties. $LaMnO_3$ delivered a maximum power density higher than 13.9 mWm^{-2} in the two-chambered MFC, a value that is twice as high as that of carbon cloth (CC) used as a cathode in similar circumstances. The internal resistance of these MFCs with different ORR cathodes was recorded. Carbon cloth had the highest internal resistance, followed by LC, LMC and LM. The reduced internal resistance of La-based perovskites, especially LM and LMC, leads to a lower activation energy of ORR in a neutral medium, which supports the catalyst reaction [53]. Transition metal cation participation and its valency largely influence ORR and the electrocatalytic activity of the perovskite-type oxides.
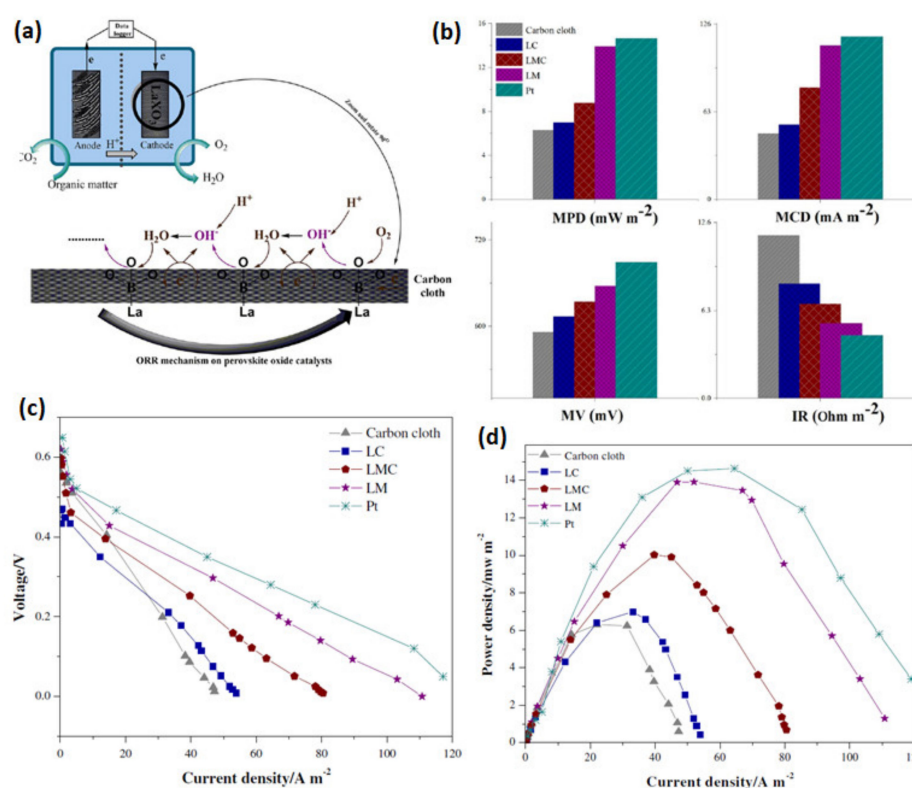
Figure 6. (**a**) Pictorial representation of ORR pathway on $LaCo_{0.5}Mn_{0.5}O_3$; (**b**) a column/bar diagram of the obtained results of the MFC with La-based perovskite catalyst in comparison with bare and Pt-coated carbon cloth cathode; (**c**) polarization curves; (**d**) power density curves of different electrodes. (Reprinted with permission from [5]. Copyright 2020, Springer, Open Access).

Xin Wang and group [53] used $La_{0.4}Ca_{0.6}Co_{0.9}Fe_{0.1}O_3$ (LCCF) perovskite, a carbon-supported Ca and Fe double-doped $LaCoO_3$. The reverse micelle technique was used to synthesize the LCCF. Finely dispersed carbon was used as a support matrix for the LCCF particles. A comparative study of the LCCF/C cathode and C cathode was conducted, using Pt as a control, at ambient temperatures and with a neutral electrolyte in a single-chambered MFC. The LCCF/C ORR catalyst followed a hybrid electron pathway of both four electrons and two electrons due to the presence of carbon. The LCCF/C perovskite oxide's structure provides oxygen vacancies and, in turn, gives oxygen mobility and reduces biofilm coverage. The advantage of the LCCF/C catalyst is that, after 15 cycles, it displays the lowest decay rate (2%) in open-circuit voltage compared to carbon (22%) and Pt (4%), proving that it can attain stable performance against biofouling (Figure 7).
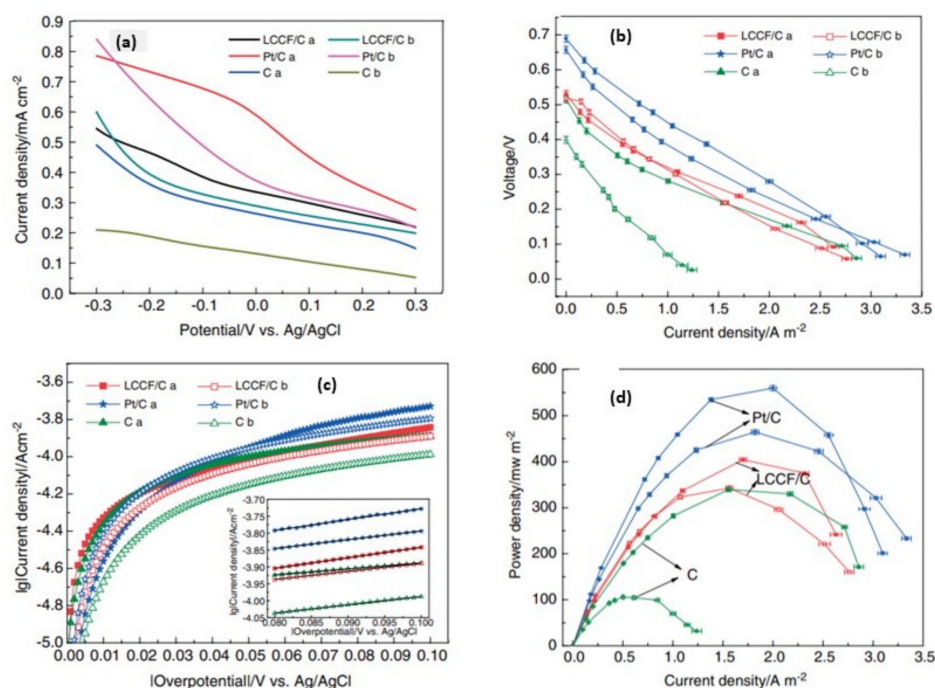
Figure 7. (**a**) Line sweep voltammograms; (**b**) MFC polarization; (**c**) Tafel plots; (**d**) curves with the three-air cathodes (50 mmol L^{-1} PBS and T = 30 °C) of LCCF/C, Pt/C and C cathodes. (Reprinted with permission from [53]. Copyright 2012, Wiley Online Library).

Farhan Papiya et al. [1] used Al_2O_3–rGO as an alternative to a platinum ORR catalyst in a single-chambered MFC. Cobalt nanoparticles of different weight percentages were added to the alumina and graphene oxide mixture. The study conducted was with four different weight percentages, along with Pt/C as a standard reference. Catalyst B, having 80 wt% of cobalt metal, was proven to show the highest power density of 548.19 mWm^{-2}. Catalyst A had 70 wt% Co, Catalyst C had 90 wt% Co and Catalyst D had 80 wt% Co but no Al_2O_3. Cyclic voltammetry and open-circuit voltage experiments proved that 80 wt% Co (Catalyst B) resulted in the highest electrocatalytic activity compared to the other catalysts. The ORR activity of the different catalysts was in the order D < C < A < Pt/C < B (Figure 8). Oxygen adsorption on the surface of the catalyst was also high for Catalyst B, proven through the BET surface test. The ratio of 80:20 (Co/Al_2O_3:rGO) worked the best out of the different catalytic materials tested on the MFC.

BaMnO$_3$ perovskite coated with carbon and its electrocatalytic properties for the oxygen evolution reaction and oxygen reduction reaction were studied by Yujiao Xu et al. [54]. A bifunctional catalyst has a wide range of applications in the field of batteries, fuel cells, etc. The study was conducted in two stages: initially, the catalytic properties of the bare BaMnO$_3$ nanorods were examined; later, the same tests were carried out with a thin layer of carbon coating on the BaMnO$_3$ nanorods. The results showed a large improvement in the peak current density, which was -0.94 mAcm^{-2} on the bare BaMnO$_3$ nanorods and -2.5 mAcm^{-2} on the carbon-coated BaMnO$_3$ nanorods. Carbon-coated BaMnO$_3$ nanorods delivered a better positive shift in the onset and half-wave potential compared with the bare BaMnO$_3$ nanorods. An electron transfer rate of 3.8 was observed in the carbon-coated BaMnO$_3$ nanorods, compared to 3.4 in the latter. The study proves that a thin layer (5%) of carbon coating can improve the stability of BaMnO$_3$ as a bifunctional catalyst (Figure 9).
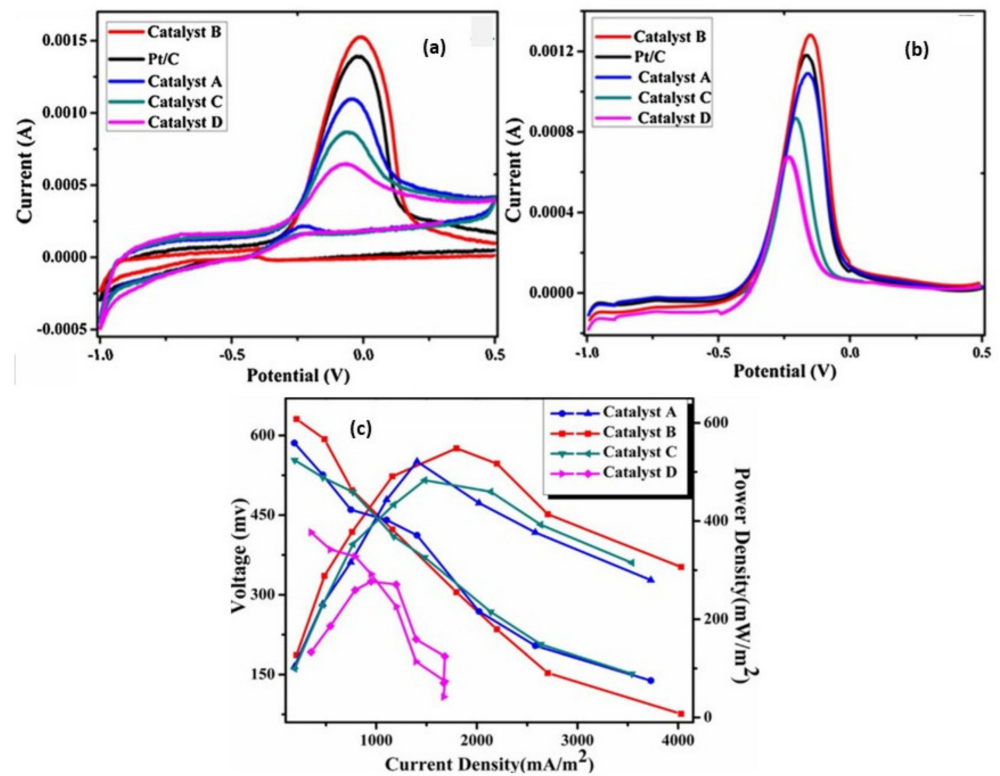
Figure 8. (**a**) Cyclic voltammograms; (**b**) LSV of Co/Al$_2$O$_3$–rGO at different wt% concentrations in a mixed bacterial culture, scan rate 10 mv/s; (**c**) polarization curve and power density curve of cathode catalysts at different Co wt%. (Reprinted with permission from [1]. Copyright 2017, Elsevier).
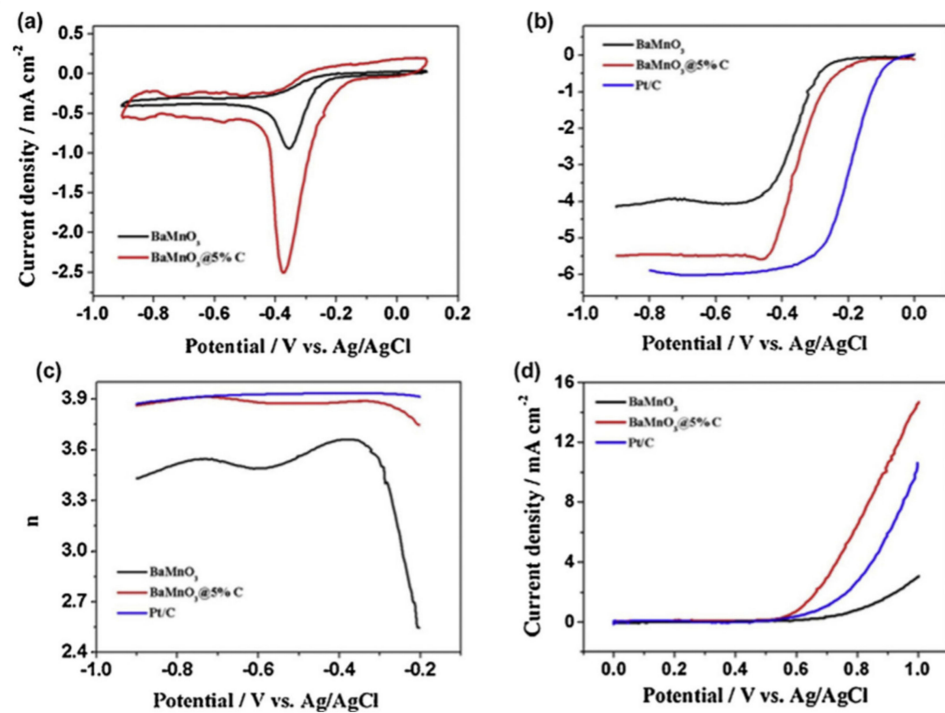
Figure 9. (**a**) Cyclic voltammetry; (**b**) linear sweep voltammogram, BaMnO$_3$ (black curve) BaMnO$_3$@ 5% C (red curve) in O$_2$ saturated 0.1 M KOH solution, commercial Pt/C (blue curve); (**c**) electron transfer rate; (**d**) LSV in N$_2$ saturated 0.1 KOH solution. (Reprinted with permission from [54]. Copyright 2015, Elsevier).

In a study conducted by L.J. Bai et al. [55], a $La_xSr_{1-x}CoO_3$ perovskite nanocatalyst was introduced as a cathode catalyst in an anaerobic fluidized bed microbial fuel cell. The experiment was carried out at different concentrations of catalyst, such as $La_{0.7}Sr_{0.3}CoO_3$, $La_{0.3}Sr_{0.5}CoO_3$ and $La_{0.8}Sr_{0.2}CoO_3$, in which $La_{0.7}Sr_{0.3}CoO_3$ produced the maximum power output of 104.59 mWm^{-2} and open-circuit voltage of 594.0 mV. The results show that $La_{0.7}Sr_{0.3}CoO_3$ achieved the best concentrations of lanthanum and strontium in the perovskite oxide, as it was more efficient in the comparative study. Table 1 summarizes the electrocatalytic properties of the various perovskite-Based Nanocomposite Electrocatalysts developed for cathodic ORR In MFCs.

Table 1. The kinetic data of Pt and the various perovskite-type oxides used in MFCs.

ORR Catalyst	Matrix	Max. Power Density	Ref. Electrode	Onset Potential	Half-Wave Potential	Number of Electrons Transferred	Current Density	Reference
Platinum	Carbon	783 mWm^{-2}	Ag/AgCl	0.158 V	−0.193 V	3.9	4.83 $mAcm^{-2}$	[52]
$CaFeZnO_3$	Carbon Cloth	892 mWm^{-2}	Ag/AgCl	0.194 V	−0.219 V	3.94	5.46 $mAcm^{-2}$	[52]
LaMnO3	Carbon Cloth	14 mWm^{-2}	Ag/AgCl	-	-	3.4	1.1 $mAcm^{-2}$	[5]
$FeMnO_3$	Graphene Oxide	166 mWm^{-2}	Ag/AgCl	-	−0.22 V	3.6	3.8 $mAcm^{-2}$	[51]
$FeMnO_3$	Carbon	460 mWm^{-2}	Ag/AgCl	-	−0.30 V	3.6	4.2 $mAcm^{-2}$	[51]
$LaCaCoFeO_3$	Carbon	405 mWm^{-2}	Ag/AgCl	-	-	-	-	[53]
$LaSrCoO_3$	Carbon	104 mWm^{-2}	Ag/AgCl	-	-	-	-	[55]
$CoAl_2O_3$	Graphene Oxide	548 mWm^{-2}	Ag/AgCl	0.13 V	−0.15 V	-	1.79 $mAcm^{-2}$	[1]
$BaMnO_3$	Carbon	790 mWm^{-2}	Ag/AgCl	0.19 V	−0.36 V	3.4	4.84 $mAcm^{-2}$	[54]

4. Summary and Perspectives

The perspective on perovskite-type oxide-based cathodes in MFCs has been discussed. The literature and the vast array of information we have on their molecular mechanisms, characteristics and behavior offer a basic understanding of perovskite cathodes. The modification of the perovskite crystal structure through doping of the A and B site has proven to be a sensible technique in improving the ORR performance. Replacing the A site with a lower-oxidation-state cation or instigating an A-site cation deficiency is indicated as a practical method to generate oxygen vacancies for ORR. The electrocatalytic properties of perovskites are also primarily dependent on the choice of B-site metal cations. The increase in ORR kinetics is associated with an optimal balance of ionic mobility, surface electron transfer and oxygen vacancies as aided by the synergistic effects of B sites. The combination of elements such as Zn and Fe will produce a synergic effect at the B site, which helps the composite to perform better and achieve excellent electricity flow rates. By introducing Zn and Co, oxygen vacancies and oxygen surface adsorption could be increased, which are beneficial to the ORR reaction by enhancing the charge transfer kinetics between the catalyst and gaseous O_2 reactants. The mesoporous and microporous composition of perovskite oxides contribute various porous channels for the exchange of electrons, and the mass transfer process is shortened. This reveals that Zn-, La- and Mn-doped perovskite-type oxides could be ideal electrocatalysts with enhanced corrosion resistance, stability and outstanding onset potential and half-wave potential. These modified perovskite oxides will display excellent ORR activity and facilitate an evident four-electron pathway that can display remarkable durability even if compared to the benchmark Pt/C catalysts. An understanding of the different reaction pathways and various key parameters influencing the perovskite oxide ORR catalysts has proven to be pivotal. In recent studies, relatively improved ORR activity has been observed for perovskite-oxide-based catalysts with carbon

added. Advancements in the field of electrocatalysis and the development of more ideal combinations of perovskite nanocatalysts will prove to be a solution for MFCs with low ORR activity and power output. This, in turn, will provide a promising replacement for the expensive Pt ORR catalyst.

References

1. Papiya, F.; Nandy, A.; Mondal, S.; Kundu, P.P. Co/Al$_2$O$_3$-rGO nanocomposite as cathode electrocatalyst for superior oxygen reduction in microbial fuel cell applications: The effect of nanocomposite composition. *Electrochim. Acta* **2017**, *254*, 1–13. [CrossRef]
2. Papiya, F.; Pattanayak, P.; Kumar, P.; Kumar, V.; Kundu, P.P. Development of highly efficient bimetallic nanocomposite cathode catalyst, composed of Ni:Co supported sulfonated polyaniline for application in microbial fuel cells. *Electrochim. Acta* **2018**, *282*, 931–945. [CrossRef]
3. Shahbazi Farahani, F.; Mecheri, B.; Reza Majidi, M.; Costa de Oliveira, M.A.; D'Epifanio, A.; Zurlo, F.; Placidi, E.; Arciprete, F.; Licoccia, S. MnOx-based electrocatalysts for enhanced oxygen reduction in microbial fuel cell air cathodes. *J. Power Sources* **2018**, *390*, 45–53. [CrossRef]
4. Fu, Z.; Yan, L.; Li, K.; Ge, B.; Pu, L.; Zhang, X. Biosensors and Bioelectronics The performance and mechanism of modi fi ed activated carbon air cathode by non-stoichiometric nano Fe$_3$O$_4$ in the microbial fuel cell. *Biosens. Bioelectron.* **2015**, *74*, 989–995. [CrossRef]
5. Nourbakhsh, F.; Mohsennia, M.; Pazouki, M. Highly efficient cathode for the microbial fuel cell using LaXO$_3$ (X = [Co, Mn, Co$_{0.5}$Mn$_{0.5}$]) perovskite nanoparticles as electrocatalysts. *SN Appl. Sci.* **2020**, *2*, 391. [CrossRef]
6. Hou, Y.; Chen, J.; He, Z. Oxygen reduction reaction catalysts used in microbial fuel cells for energy-efficient wastewater treatment: A review. *Mater. Horiz.* **2016**, *3*, 382–401. [CrossRef]
7. Ayyaru, S.; Dharmalingam, S. Bioresource Technology Development of MFC using sulphonated polyether ether ketone (SPEEK) membrane for electricity generation from waste water. *Bioresour. Technol.* **2011**, *102*, 11167–11171. [CrossRef] [PubMed]
8. Sivasankaran, A.; Sangeetha, D.; Ahn, Y. Nanocomposite membranes based on sulfonated polystyrene ethylene butylene polystyrene (SSEBS) and sulfonated SiO$_2$ for microbial fuel cell application. *Chem. Eng. J.* **2016**, *289*, 442–451. [CrossRef]
9. Ayyaru, S.; Letchoumanane, P.; Dharmalingam, S.; Raj, A. Performance of sulfonated polystyrene e ethylene e butylene e polystyrene membrane in microbial fuel cell for bioelectricity production. *J. Power Sources* **2012**, *217*, 204–208. [CrossRef]
10. Ayyaru, S.; Dharmalingam, S. A study of in fl uence on nanocomposite membrane of sulfonated TiO$_2$ and sulfonated polystyrene-ethylene-butylene-polystyrene for microbial fuel cell application. *Energy* **2015**, *88*, 202–208. [CrossRef]
11. Peera, S.G.; Maiyalagan, T.; Liu, C.; Ashmath, S.; Lee, T.G.; Jiang, Z.; Mao, S. A review on carbon and non-precious metal based cathode catalysts in microbial fuel cells. *Int. J. Hydrogen Energy* **2021**, *46*, 3056–3089. [CrossRef]
12. Mishra, P.; Lee, J.; Kumar, D.; Lauro, R.O.; Costa, N.; Pathania, D.; Kumar, S.; Lee, J.; Singh, L. Engineered Nanoenzymes with Multifunctional Properties for Next-Generation Biological and Environmental Applications. *Adv. Funct. Mater.* **2021**, *2021. 23*, 200–220. [CrossRef]
13. Nourbakhsh, F.; Pazouki, M.; Mohsennia, M. Impact of modified electrodes on boosting power density of microbial fuel cell for effective domestic wastewater treatment: A case study of Tehran. *J. Fuel Chem. Technol.* **2017**, *45*, 871–879. [CrossRef]
14. Peera, S.G.; Liu, C.; Sahu, A.K.; Selvaraj, M.; Rao, M.; Lee, T.G.; Koutavarapu, R.; Shim, J.; Singh, L. Recent Advances on Mxene-Based Electrocatalysts toward Oxygen Reduction Reaction: A focused Review. *Adv. Mater. Interfaces* **2021**, *8*, 28. [CrossRef]
15. Erikson, H.; Sarapuu, A.; Tammeveski, K. Oxygen Reduction Reaction on Silver Catalysts in Alkaline Media: A Minireview. *ChemElectroChem* **2019**, *6*, 73–86. [CrossRef]
16. Fan, Y.; Sharbrough, E.; Liu, H. Quantification of the internal resistance distribution of microbial fuel cells. *Environ. Sci. Technol.* **2008**, *42*, 8101–8107. [CrossRef] [PubMed]
17. Chen, T.; Kalimuthu, P.; Anushya, G.; Chen, S.; Ramachandran, R.; Mariyappan, V.; Muthumala, D.C. Nanocomposite for Oxygen Evolution and Oxygen Reduction Reaction: An Overview. *Materials* **2021**, *14*, 2976. [CrossRef]
18. Liu, J.; Mater, J.P.; Liu, J.; Ma, J.; Zhang, Z.; Qin, Y.; Wang, Y.; Wang, Y.; Tan, R.; Duan, X.; et al. Roadmap: Electrocatalysts for green catalytic processes Journal of Physics: Materials OPEN ACCESS 2021 Roadmap: Electrocatalysts for green catalytic processes. *J. Phys. Mater.* **2021**, *4*, 022004. [CrossRef]

19. Li, M.; Zhou, J.; Bi, Y.G.; Zhou, S.Q.; Mo, C.H. Transition metals (Co, Mn, Cu) based composites as catalyst in microbial fuel cells application: The effect of catalyst composition. *Chem. Eng. J.* **2020**, *383*, 123152. [CrossRef]
20. Kodali, M.; Santoro, C.; Serov, A.; Kabir, S.; Artyushkova, K.; Matanovic, I.; Atanassov, P. Air breathing cathodes for microbial fuel cell using Mn-, Fe-, Co- and Ni-containing platinum group metal-free catalysts. *Electrochim. Acta* **2017**, *231*, 115–124. [CrossRef]
21. Türk, K.K.; Kruusenberg, I.; Kibena-Põldsepp, E.; Bhowmick, G.D.; Kook, M.; Tammeveski, K.; Matisen, L.; Merisalu, M.; Sammelselg, V.; Ghangrekar, M.M.; et al. Novel multi walled carbon nanotube based nitrogen impregnated Co and Fe cathode catalysts for improved microbial fuel cell performance. *Int. J. Hydrogen Energy* **2018**, *43*, 23027–23035. [CrossRef]
22. Zhang, F.; Cheng, S.; Pant, D.; Van Bogaert, G.; Logan, B.E. Electrochemistry Communications Power generation using an activated carbon and metal mesh cathode in a microbial fuel cell. *Electrochem. Commun.* **2009**, *11*, 2177–2179. [CrossRef]
23. Paper, R. Electrode materials for microbial fuel cells: Nanomaterial approach. *Mater. Renew. Sustain. Energy* **2015**, *4*, 21–31. [CrossRef]
24. Yuan, H.; He, Z. Graphene-modified electrodes for enhancing the performance of microbial fuel cells. *Nanoscale* **2015**, *7*, 7022–7029. [CrossRef]
25. Tan, L.; Liu, Z.Q.; Li, N.; Zhang, J.Y.; Zhang, L.; Chen, S. CuSe decorated carbon nanotubes as a high performance cathodecatalyst for microbial fuel cells. *Electrochim. Acta* **2016**, *213*, 283–290. [CrossRef]
26. Wang, X.; Yuan, C.; Shao, C.; Zhuang, S.; Ye, J.; Li, B. Enhancing oxygen reduction reaction by using metal-free nitrogen-doped carbon black as cathode catalysts in microbial fuel cells treating wastewater. *Environ. Res.* **2020**, *182*, 109011. [CrossRef] [PubMed]
27. Malyan, S.K.; Kumar, S.S.; Kishor, R.; Ghosh, P.; Kumar, A.; Singh, R.; Singh, L. Biochar for environmental sustainability in the energy-water-agroecosystem nexus. *Renew. Sustain. Energy Rev.* **2021**, *149*, 111379. [CrossRef]
28. Li, S.; Ho, S.; Hua, T.; Zhou, Q.; Li, F.; Tang, J. Sustainable biochar as an electrocatalysts for the oxygen reduction reaction in microbial fuel cells. *Green Energy Environ.* **2021**, *6*, 644–659. [CrossRef]
29. Allam, F.; Elnouby, M.; El-khatib, K.M. ScienceDirect Water hyacinth (*Eichhornia crassipes*) biochar as an alternative cathode electrocatalyst in an air-cathode single chamber microbial fuel cell. *Int. J. Hydrogen Energy* **2019**, *45*, 5911–5927. [CrossRef]
30. Li, Y.; Li, Q.; Wang, H.; Zhang, L.; Wilkinson, D.P.; Zhang, J. Recent Progresses in Oxygen Reduction Reaction Electrocatalysts for Electrochemical Energy Applications. *Electrochem. Energy Rev.* **2019**, *2*, 518–538. [CrossRef]
31. Ayyaru, S.; Mahalingam, S.; Ahn, Y. A non-noble V_2O_5 nanorods as an alternative cathode catalyst for microbial fuel cell applications. *Int. J. Hydrogen Energy* **2019**, *44*, 4974–4984. [CrossRef]
32. Goswami, C.; Hazarika, K.K.; Bharali, P. Transition metal oxide nanocatalysts for oxygen reduction reaction. *Mater. Sci. Energy Technol.* **2018**, *1*, 117–128. [CrossRef]
33. Wang, Z.-L.; Xu, D.; Xu, J.-J.; Zhang, X.-B. Oxygen electrocatalysts in metal–air batteries: from aqueous to nonaqueous electrolytes. *Chem. Soc. Rev.* **2014**, *43*, 7746–7786. [CrossRef] [PubMed]
34. Dong, C.; Liu, Z.W.; Liu, J.Y.; Wang, W.C.; Cui, L.; Luo, R.C.; Guo, H.L.; Zheng, X.L.; Qiao, S.Z.; Du, X.W.; et al. Modest Oxygen-Defective Amorphous Manganese-Based Nanoparticle Mullite with Superior Overall Electrocatalytic Performance for Oxygen Reduction Reaction. *Small* **2017**, *13*, 1603903. [CrossRef]
35. Zhang, T.; He, C.; Sun, F.; Ding, Y.; Wang, M.; Peng, L.; Wang, J.; Lin, Y. Co_3O_4 nanoparticles anchored on nitrogen-doped reduced graphene oxide as a multifunctional catalyst for H_2O_2 reduction, oxygen reduction and evolution reaction. *Sci. Rep.* **2017**, *7*, 43638. [CrossRef]
36. Xiao, J.; Kuang, Q.; Yang, S.; Xiao, F.; Wang, S.; Guo, L. Surface Structure Dependent Electrocatalytic Activity of Co_3O_4 Anchored on Graphene Sheets toward Oxygen Reduction Reaction. *Sci. Rep.* **2013**, *3*, 2300. [CrossRef]
37. Mahalingam, S.; Ayyaru, S.; Ahn, Y. Chemosphere Facile one-pot microwave assisted synthesis of rGO-CuS-ZnS hybrid nanocomposite cathode catalysts for microbial fuel cell application. *Chemosphere* **2021**, *278*, 130426. [CrossRef]
38. Zhou, X.; Xu, Y.; Mei, X.; Du, N.; Jv, R.; Hu, Z.; Chen, S. Polyaniline/β-MnO_2 nanocomposites as cathode electrocatalyst for oxygen reduction reaction in microbial fuel cells. *Chemosphere* **2018**, *198*, 482–491. [CrossRef]
39. Dong, A.; Lee, U.; Li, J.; Park, M.G.; Seo, M.H.; Stadelmann, I.; Ricardez-sandoval, L.; Un, D.; Li, J.; Gyu, M.; et al. Self-assembly of Spinel Nano-crystals into Mesoporous Spheres as Bi-functionally Active Oxygen Reduction and Evolution Electrocatalysts. *ChemSusChem* **2017**, *10*, 2258–2266. [CrossRef]
40. Bu, Y.; Jang, H.; Gwon, O.; Kim, S.H.; Joo, S.H.; Nam, G.; Kim, S.; Qin, Y.; Zhong, Q.; Kwak, S.K.; et al. Synergistic interaction of perovskite oxides and N-doped graphene in versatile electrocatalyst. *J. Mater. Chem. A* **2019**, *7*, 2048–2054. [CrossRef]
41. Dzara, M.J.; Christ, J.M.; Joghee, P.; Ngo, C.; Cadigan, C.A.; Bender, G.; Richards, R.M.; Hayre, R.O.; Pylypenko, S. La and Al co-doped $CaMnO_3$ perovskite oxides: From interplay of surface properties to anion exchange membrane fuel cell performance. *J. Power Sources* **2018**, *375*, 265–276. [CrossRef]
42. Wang, X.T.; Ouyang, T.; Wang, L.; Zhong, J.H.; Liu, Z.Q. Surface Reorganization on Electrochemically-Induced Zn–Ni–Co Spinel Oxides for Enhanced Oxygen Electrocatalysis. *Angew. Chem.* **2020**, *132*, 6554–6561. [CrossRef]
43. Onrubia-Calvo, J.A.; Pereda-Ayo, B.; González-Velasco, J.R. Perovskite-Based Catalysts as Efficient, Durable, and Economical NOx Storage and Reduction Systems. *Catalysts* **2020**, *10*, 208. [CrossRef]
44. Kumar, A.; Kumar, A.; Krishnan, V. Perovskite Oxide Based Materials for Energy and Environment-Oriented Photocatalysis. *ACS Catal.* **2020**, *10*, 10253–10315. [CrossRef]
45. Fierro, J.L.G. Chemical Structures and Performance of Perovskite Oxides. *Chem. Rev.* **2017**, *101*, 1981–2018.

46. Suntivich, J.; Gasteiger, H.A.; Yabuuchi, N.; Nakanishi, H.; Goodenough, J.B.; Shao-Horn, Y. Design principles for oxygen-reduction activity on perovskite oxide catalysts for fuel cells and metal-air batteries. *Nat. Chem.* **2011**, *3*, 546–550. [CrossRef] [PubMed]
47. Beall, C.E.; Fabbri, E.; Schmidt, T.J. Perovskite Oxide Based Electrodes for the Oxygen Reduction and Evolution Reactions: The Underlying Mechanism. *ACS Catal.* **2021**, *11*, 3094–3114. [CrossRef]
48. Risch, M. Perovskite electrocatalysts for the Oxygen reduction reaction in alkaline media. *Catalysts* **2017**, *7*, 154. [CrossRef]
49. Xue, Y.; Sun, S.; Wang, Q.; Dong, Z.; Liu, Z. Transition metal oxide-based oxygen reduction reaction electrocatalysts for energy conversion systems with aqueous electrolytes. *J. Mater. Chem. A* **2018**, *6*, 10596–10626. [CrossRef]
50. Ji, Q.; Bi, L.; Zhang, J.; Cao, H.; Zhao, X.S. The role of oxygen vacancies of ABO_3 perovskite oxides in the oxygen reduction reaction. *Energy Environ. Sci.* **2020**, *13*, 1408–1428. [CrossRef]
51. Shahbazi Farahani, F.; Mecheri, B.; Majidi, M.R.; Placidi, E.; D'Epifanio, A. Carbon-supported Fe/Mn-based perovskite-type oxides boost oxygen reduction in bioelectrochemical systems. *Carbon* **2019**, *145*, 716–724. [CrossRef]
52. Dai, Y.; Li, H.; Wang, Y.; Zhong, K.; Zhang, H.; Yu, J.; Huang, Z.; Yan, J.; Huang, L.; Liu, X.; et al. Zn-doped $CaFeO_3$ perovskite-derived high performed catalyst on oxygen reduction reaction in microbial fuel cells. *J. Power Sources* **2021**, *489*, 229498. [CrossRef]
53. Dong, H.; Yu, H.; Wang, X.; Zhou, Q.; Sun, J. Carbon-supported perovskite oxides as oxygen reduction reaction catalyst in single chambered microbial fuel cells. *J. Chem. Technol. Biotechnol.* **2013**, *88*, 774–778. [CrossRef]
54. Xu, Y.; Tsou, A.; Fu, Y.; Wang, J.; Tian, J.H.; Yang, R. Carbon-Coated Perovskite $BaMnO_3$ Porous Nanorods with Enhanced Electrocatalytic Perporites for Oxygen Reduction and Oxygen Evolution. *Electrochim. Acta* **2015**, *174*, 551–556. [CrossRef]
55. Bai, L.; Wang, X.; He, H. Preparation and characteristics of LAXSR1-XCOO3 as cathode catalysts for microbial fuel cell. In *Particle Science and Engineering, Proceedings of UK–China International Particle Technology Forum IV*; The Royal Society of Chemistry: London, UK, 2014; pp. 15–21, ISBN 9781849739573.